

Thermodynamical approaches to efficient sympathetic cooling in ultracold Fermi-Bose atomic mixtures

Michael Brown-Hayes,¹ Qun Wei,¹ Carlo Presilla,^{2,3,4} and Roberto Onofrio^{5,3,1}

¹Department of Physics and Astronomy, Dartmouth College, 6127 Wilder Laboratory, Hanover, NH 03755

²Dipartimento di Fisica, Università di Roma "La Sapienza", Piazzale A. Moro 2, Roma 00185, Italy

³Center for Statistical Mechanics and Complexity, INFN - CNR, Unità di Roma 1, Roma 00185, Italy

⁴INFN, Sezione di Roma 1, Roma 00185, Italy

⁵Dipartimento di Fisica "Galileo Galilei", Università di Padova, Via Marzolo 8, Padova 35131, Italy

(Dated: February 20, 2024)

We discuss the cooling efficiency of ultracold Fermi-Bose mixtures in species-selective traps using a thermodynamical approach. The dynamics of evaporative cooling trajectories is analyzed in the specific case of bichromatic optical dipole traps also taking into account the effect of partial spatial overlap between the Fermi gas and the thermal component of the Bose gas. We show that large trapping frequency ratios between the Fermi and the Bose species allow for the achievement of a deeper Fermi degeneracy, consolidating in a thermodynamical setting earlier arguments based on more restrictive assumptions. In particular, we confirm that the minimum temperature of the mixture is obtained at the crossover between boson and fermion heat capacities, and that below such a temperature sympathetic cooling vanishes. When the effect of partial overlap is taken into account, optimal sympathetic cooling of the Fermi species may be achieved by properly tuning the relative trapping strength of the two species in a time-dependent fashion. Alternatively, the dimensionality of the trap in the final stage of cooling can be changed by increasing the confinement strength, which also results in a crossover of the heat capacities at deeper Fermi degeneracies. This technique may be extended to Fermi-Bose degenerate mixtures in optical lattices.

PACS numbers: 03.75.Ss, 51.30.+i, 32.80.Pj, 67.60.-g

I. INTRODUCTION

Atomic physics and condensed matter physics now enjoy strong connections through the study of quantum transport in ultracold dilute gases [1]. Long-standing problems of condensed matter physics may be addressed by preparing controllable environments for the dynamics of cold atoms and by continuously tuning their interactions. This in turn allows for the study of fundamental features of high-temperature superconductivity using ultracold gases as controllable, analog computers of various model hamiltonians [2].

Degenerate Fermi gases were first produced in 1999 [3], and more recently Fermi superfluid behaviour has been conclusively evidenced through the generation of vortices [4] and the onset of critical velocities [5] in degenerate samples of ^6Li . Weakly interacting Fermi gases are difficult to bring to quantum degeneracy mainly due to fundamental obstacles in adapting cooling techniques successfully used for bosonic species. In particular, the Pauli principle inhibits efficient evaporative cooling among identical fermions as they reach degeneracy. This issue has been circumvented by developing two cooling techniques, namely mutual evaporative cooling of fermions prepared in two different states and sympathetic cooling with a Bose species. In the case of dual evaporative cooling, a selective removal of the most energetic fermions in both the hyperfine states is performed. Provided that the initial number of atoms in each state is roughly the same, efficient dual evaporative cooling can be performed throughout the entire process. Limits to

the minimum reachable absolute temperature using dual evaporative cooling have been addressed in [6], resulting in a minimum reachable temperature $T' = k_B$, with the chemical potential of the Fermi gas (see also [7] for a complementary analysis). Moreover, the number of available atoms N_f progressively decreases over time with a corresponding drop in the Fermi temperature T_F proportional to $N_f^{1/3}$. The resulting gain in terms of a lower $T = T_F$ degeneracy ratio is therefore limited, and the smaller clouds obtained at the end of the evaporative cooling are detrimental to detailed experimental investigations requiring a large number of atoms, such as a quantitative mapping of the superfluid phases. In the case of sympathetic cooling using a Bose gas, the number of fermions is instead kept constant, leaving aside losses due to background pressure and two- and three-body collisions, and the cooling efficiency depends on the optimization of Fermi and Bose collisional properties, heat capacities, and, in the case of inhomogeneous samples, their spatial overlap.

To date, the smallest Fermi degeneracy achieved with both cooling techniques is in the $T = T_F \sim 5 \cdot 10^2$ range [8, 9]. This limitation has not precluded the study of temperature-independent features of degenerate Fermi gases, such as quantum phase transitions related to unbalanced spin populations [10, 11, 12, 13] or the effect of Fermi impurities in the coherence properties of a Bose gas [14, 15]. However, the study of more conventional phase transitions in which the temperature is the key parameter is still uncharted territory and, as discussed for instance in [16, 17, 18], this requires the achievement

of degeneracy factors $T=T_F \ll 10^{-3}$ or lower. Unconventional pairing mechanisms that are unstable at higher $T=T_F$ could then be observed, and the phase diagram of Fermi atoms in the degenerate regime could be mapped in a wider range of parameter space. Moreover, the study of ultracold Fermi-Bose mixtures is an interesting subject in itself, acting as the counterpart of the ^3He - ^4He liquid mixtures extensively investigated at much higher densities and temperatures.

Considering the novel physical insights that deeper Fermi degenerate gases and Fermi-Bose mixtures may provide, it is relevant to discuss the limitations to reaching the lowest $T=T_F$ in realistic settings available by means of sympathetic cooling, and ways to overcome them. Here, we discuss two different techniques to overcome the apparent $T=T_F \ll 10^{-2}$ limit observed so far, based on optimized heat capacity matching with species-selective traps or with lower dimensionality traps. The paper is organized as follows. In Section II, after briefly reviewing previous results on sympathetic cooling in species-selective traps, we determine the time evolution of the temperature of the mixture in a particular class of species-selective traps through a thermodynamical analysis, and we subsequently include the effect of the spatial overlap between the thermal component of the Bose gas and the Fermi gas. The main novelty with respect to previous semiquantitative analyses is that including both temporal and spatial dependence in the thermodynamics of sympathetic cooling leads to an optimization of the heat capacity provided that a time-dependent trapping frequency ratio is implemented. As an alternative to this optimization procedure, in Section III we discuss heat capacity matching resulting from lower effective dimensions for trapping, exploiting the strong dependence on dimensionality of the density of states of the Bose gas. A simpler protocol for optimizing heat capacity is available with nearly one-dimensional Fermi-Bose mixtures, which requires time modulation of the trapping strengths of the Fermi and Bose gases in the last cooling stage. Broader considerations on generic trapping settings are then discussed in the conclusions.

II. HEAT CAPACITY MATCHING THROUGH SPECIES-SELECTIVE TRAPPING

After discussing the evidence for a correlation between the degeneracy factor $T=T_F$ and the trapping frequency ratio between the Fermi and the Bose species, we review previous results on the use of species-selective traps and their limiting assumptions. We then relax these assumptions with a thermodynamical analysis also including the effect of the partial overlap between the Fermi gas and the thermal component of the Bose gas in the specific case of bichromatic traps.

A. Qualitative considerations on heat capacity matching

Evaporative cooling has been instrumental in reaching Bose degeneracy for dilute atomic gases. Extensive analysis have already addressed the dynamics of evaporative cooling of a Bose gas [19, 20, 21, 22], using Monte-Carlo [23, 24], mean-field analysis [25], and beyond [26], including also more detailed effects [27, 28, 29]. These studies have been also extended to the case of separate Bose and Fermi clouds [30] or Fermi-Bose mixtures using the quantum Boltzmann equation [31] or other semiclassical models [32]. Some generic features of the effectiveness in cooling fermions through a Bose gas can be addressed based on the insights first discussed in [3] and then analyzed in more detail in [34, 35]. The heat capacity of a degenerate Fermi gas depends linearly on its temperature, being for a harmonically trapped gas equal to $C_F \propto k_B N_F T=T_F$, while a harmonically trapped degenerate Bose gas has a cubic dependence on temperature $C_B \propto 10.8 k_B N_B (T=T_C)^3$. The degeneracy parameter can be written in terms of the ratio of heat capacities: $T=T_F \propto 0.35 (!_B=!_F)^{3/2} (C_B=C_F)^{1/2}$ [35]. By assuming that sympathetic cooling loses efficiency when the heat capacity of the Bose gas matches exactly that of the Fermi gas ($C_B = C_F$) we obtain a conservative limit on the attainable $T=T_F$ vs. $!_F=!_B$ space, depicted in Fig. 1 by the upper line. In the hypothesis that some residual cooling occurs when $C_B < C_F$, for instance with cooling stopping when $C_B=C_F \approx 0.1$, we obtain the lower line in Fig. 1. Realistically, we do expect that sympathetic cooling will be quenched when $0.1 < C_B=C_F < 1$, i.e. in the region delimited by the two lines. In Fig. 1 we also plot the minimum $T=T_F$ as obtained by the various running experiments with Fermi-Bose mixtures. Although the number of explored Fermi-Bose mixtures is limited and the diverse technical solutions for trapping and cooling may provide alternative explanations [36], a correlation between the trapping frequency ratio $!_F=!_B$ and the minimum achieved $T=T_F$ seems corroborated by the actual results and invites more quantitative attention. Further analysis provided insight into the cooling limitations in different trapping conditions and for different species combinations [41]. It was found that significant gains in $T=T_F$ could be achieved for stronger relative Fermi-Bose confinements than the natural $!_F=!_B$ provided by the mass ratio between the two species. In [41] the focus was on an equilibrium situation at nearly zero temperature, and to develop a more comprehensive understanding of the cooling process a dynamical framework is needed in which crucial finite temperature effects for the Bose gas are taken into account. Here we specialize the analysis of the thermodynamics as ^6Li is sympathetically cooled by evaporating ^{87}Rb in an optical dipole trap. This mixture, expected to optimize cooling efficiency [41, 42], is currently used in various laboratories [43, 44, 45] both for studies of Fermi superfluidity and for the formation of ultracold molecules [46], taking

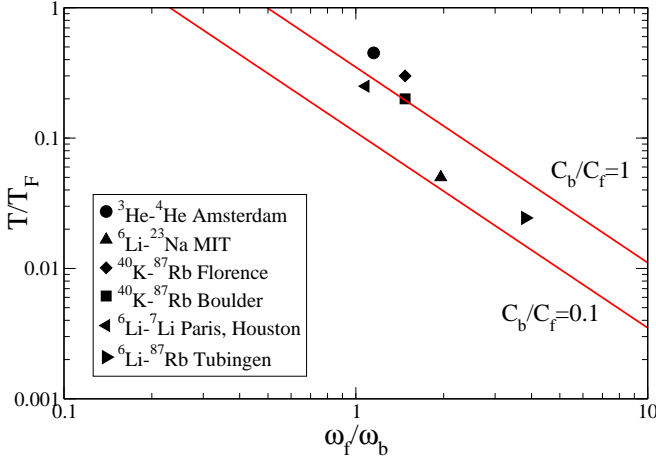


FIG. 1: (Color online) Plot of experimentally obtained $T=T_F$ versus the trapping frequency ratio ω_f/ω_b . Lines indicate the theoretically predicted range of $T=T_F$ values based on a semi-quantitative heat capacity matching argument as discussed in the text. The experimental data are taken from [37] (Amsterdam), [8] (MIT), [38] (Florence), [40] (Boulder), [33] (Houston), [39] (Paris), [43] (Tubingen).

advantage of the large electric dipole moment of Li-Rb molecules [47].

In all previous discussions of species-selective traps a static picture was assumed for the cooling of the Fermi-Bose mixture, relying on the analysis already available in the case of single-species trapping [48]. A critical element of this cooling is to balance the thermalization and loss rates; rapid trap modification allows for minimization of atom losses but is limited by the requirement that we go proceed slowly enough to keep the system at thermal equilibrium. It has been shown [49] that thermodynamic equilibrium is maintained if the ratio between the potential depth and the atomic cloud temperature, given by

$U=k_B T$, is kept constant. The time-dependence of the potential depth is then given by [48]:

$$\frac{U(t)}{U_i} = 1 + \frac{t}{\tau_e} \quad (1)$$

where U_i is the initial potential depth, $\tau_e = 2(\gamma_0/3) = \gamma_0$, and $\gamma_1 = (2/3)\gamma_0(1/4)\exp(-\gamma_0/4)$, with $\gamma_0 = \gamma_1 + (\gamma_2/5) = (\gamma_2/4)$ and γ_1 the initial elastic collision rate. With the time dependence of U determined in this way we can obtain the other relevant quantities in the process (number of particles, temperature, density, scattering rates) resulting in scaling laws similar to Eq. (1). A potential depth/temperature ratio of ≈ 5 to 10 is considered to yield optimal efficiency in evaporative cooling [49]. This approach can be applied to either the simple case of evaporative cooling of a single Bose species, or the sympathetic cooling in a Fermi-Bose mixture. In both cases, Eq. (1) describes the potential depth of the Bose species U_b , with the implicit assumption that the presence of the fermions does not drastically affect the

evaporation and cooling of the bosons. This is justified since all dual-species systems trap at least an order of magnitude more bosons than fermions, but this approximation may suffer towards the end of the cooling process when a majority of the bosons have been evaporated.

In the case of a bichromatic optical dipole trap, from U_b we determine the required power P_1 of the laser concerning both species, and then for a targeted trapping strength ratio ω_f/ω_b we can calculate the required power P_2 for the Bose-decoulping laser, and finally determine the fermion potential depth U_f . In this way we have independent control of the spatial size and potential depth for each of the two species, allowing us to either maintain a constant ω_f/ω_b throughout cooling or adjust the relative trapping strengths during the process.

The exact way in which the temperature is determined from the trapping parameters depends upon both the model and the proposed cooling strategy. Eq. (1) merely identifies a limit to the cooling rate if thermodynamic equilibrium is to be maintained throughout the process, and assuming a constant ratio, as it was discussed in [34]. In practice, these assumptions can be relaxed by using a more dynamical model based on energy balance, as we discuss in the next section.

B. Thermodynamic balance

To move beyond the limiting assumptions in [34], we start our analysis by considering a dual-species system at thermodynamic equilibrium. The trap parameters are then suddenly changed in order to force some bosons to evaporate; then one waits for a new thermodynamic equilibrium before applying another evaporation step, in analogy to the scheme discussed in [50]. The step-by-step temperature reached in this way is determined by energy conservation for the Fermi and Bose gases [51].

For concreteness, we consider a species-selective trapping scheme as described in [52]. A mixture of N_f fermions and N_b bosons is confined into a bichromatic optical dipole trap tailored by two lasers of wavelengths λ_1, λ_2 and powers P_1, P_2 . In order to obtain quasi-analytic results, we will approximate the trap potential by a truncated harmonic potential properly reproducing the bottom curvature and the depth of the well. This approximation becomes exact for energies small with respect to the trap depth, a condition satisfied in the cases discussed below. The presence of the second laser allows one to make the trap parameters of the fermion species, namely the characteristic frequencies $\omega_{fx}, \omega_{fy}, \omega_{fz}$ and the depth U_f , different from the corresponding boson parameters, $\omega_{bx}, \omega_{by}, \omega_{bz}$ and U_b . As a consequence, the ratio ω_f/ω_b , for each species $s = b, f$ we define $\omega_s = (\omega_{sx}, \omega_{sy}, \omega_{sz})^{1/3}$, can be varied from its mass-determined value for $P_2/P_1 = 0$ to an ideally arbitrary large value for P_2/P_1 approaching a positive critical value [52]. The evaporation steps are carried out by decreasing the power P_1 of the reference laser while maintaining the

ratio $P_2=P_1$ at a constant value. In this way, the trap depths U_b, U_f , which are proportional to P_1 , and the frequencies ω_b, ω_f (proportional to P_1), decrease while the ratio $\omega_f=\omega_b$ remains constant [53].

At the end of an evaporation step in which the power of the reference laser is changed from P_1 to $P_1 + dP_1$ and once thermodynamic equilibrium is reestablished, the temperature changes from T to $T + dT$ according to an energy balance equation of the form

$$(U_b + k_B T) dN_b^{\text{ex}} = dE_b + dE_f ; \quad (2)$$

where dN_b^{ex} is the number of bosons in the excited states at temperature T that evaporate and $U_b + k_B T$ (with 0 1) is the mean energy per evaporated boson [20]. The quantities dE_b and dE_f are the energy changes of the trapped boson and fermion species, both at temperature T .

By observing that due to a change of P_1 , all the quan-

tities $T, \omega_b, U_b, \omega_f, U_f$ change and using for N_b^{ex}, E_b and E_f the expressions provided by Eqs. (A 9), (A 8) and (A 12), we have

$$dN_b^{\text{ex}} = \frac{\partial N_b^{\text{ex}}}{\partial T} dT + \frac{\partial N_b^{\text{ex}}}{\partial \omega_b} d\omega_b + \frac{\partial N_b^{\text{ex}}}{\partial U_b} dU_b ; \quad (3)$$

$$dE_b = \frac{\partial E_b}{\partial T} dT + \frac{\partial E_b}{\partial \omega_b} d\omega_b + \frac{\partial E_b}{\partial U_b} dU_b ; \quad (4)$$

$$dE_f = \frac{\partial E_f}{\partial T} dT + \frac{\partial E_f}{\partial \omega_f} d\omega_f ; \quad (5)$$

It is worth to point out that, within the approximation used, E_f does not depend on U_f and the number of fermions N_f remains constant. By evaluating the above partial derivatives and inserting the result into Eq. (2), we arrive at

$$\frac{dT}{dP_1} = \frac{\frac{T}{T_F} \frac{3}{2} \frac{\omega_f}{\omega_b}^3 \frac{T}{T_F}^2 P_1 \frac{U_b P_1^{1=2}}{k_B T_F} \frac{T}{T_F}^1 P_1^{1=2} + \frac{1}{2} + \frac{3}{4} \frac{T}{T_F}^2}{\frac{3}{2} \frac{\omega_f}{\omega_b}^3 \frac{T}{T_F}^2 q \frac{U_b P_1^{1=2}}{k_B T_F} \frac{T}{T_F}^1 P_1^{1=2} 1} ; \quad (6)$$

where we used $d(T=T_F) = dT=T_F (T=T_F) dT_F=T_F$ and $dT_F=T_F = dP_1=(2P_1)$, which stems from the proportionality of T_F to ω_f , namely $k_B T_F = (6N_f)^{1=3} \sim \omega_f$, see Eq. (A 13). Like $\omega_f=\omega_b$, the value of $U_b P_1^{1=2}=k_B T_F$ is a constant determined by the value of the ratio $P_2=P_1$, and $p(x)$ and $q(x)$ are defined as

$$p(x) = \int_0^x \frac{t^3}{e^t - 1} dt + \frac{x^3}{e^x - 1} ; \quad (7)$$

$$q(x) = 3x \int_0^x \frac{t^2}{e^t - 1} dt - 4 \int_0^x \frac{t^3}{e^t - 1} dt + 3 \int_0^x \frac{t^2}{e^t - 1} dt - \frac{x^3}{e^x - 1} ; \quad (8)$$

Note that $p(0) = q(0) = 0$ whereas $p(x) \sim 6(4)$ and $q(x) \sim 6(3)x - 24(4) + 6(3)$ for $x \rightarrow 1$, being the Riemann zeta function.

Equation (6) is a nonlinear ordinary differential equation which allows for the determination of $T=T_F(P_1)$ during the evaporative cooling. Observing that both functions $p(x)$ and $q(x)$ are non negative for $x \geq 0$ and assuming for simplicity $\omega_f=\omega_b$, the qualitative behavior of $T=T_F(P_1)$ is as follows. The numerator of the last fraction in Eq. (6) is always positive. If we start from initial values of P_1 and $T=T_F$ respectively not too small and not too large, the argument of the functions p and q is large with respect to unity, which is equivalent to state that $U_b = k_B T$, a fact that also justifies the

choice $\omega_f=\omega_b$. The denominator of the last fraction in Eq. (6) is thus also positive so that $T=T_F$ decreases by decreasing P_1 . The decrease may be faster or slower than $P_1^{1=2}$ depending on the value of the constants $\omega_f=\omega_b$ and $U_b P_1^{1=2}=k_B T_F$. Eventually, however, the last fraction in Eq. (6) becomes larger than 1 so that a second regime starts in which $T=T_F$ decreases faster and faster. As a consequence, the argument of the functions p and q decreases and the denominator of the last fraction in Eq. (6) approaches 0. A singular point is thus reached in which $d(T=T_F)/dP_1 = 1$ and $T=T_F > 0$. A numerical study also shows that Eq. (6) has a discontinuity at the singular point with unphysical negative values of $T=T_F$ on the left. The value of $T=T_F$ at the right of the singular point represents the minimum achievable $T=T_F$ during the cooling, provided that the initial number of bosons is sufficiently large so that they are not completely evaporated before the singular point is reached.

The behavior of $T=T_F$ as a function of P_1 is shown in Fig. 2 for different initial conditions and different values of $\omega_f=\omega_b$. We stress that whereas the minimum $T=T_F$ depends very little on the details of the cooling, the number of atoms of both species and initial values of temperature and reference laser power, we observe a substantial decrease of the minimum achievable $T=T_F$, by increasing the ratio $\omega_f=\omega_b$. This is in agreement with a previous prediction based on a rough matching of boson and fermion heat capacities [34]. In fact, the singular point of Eq. (6)

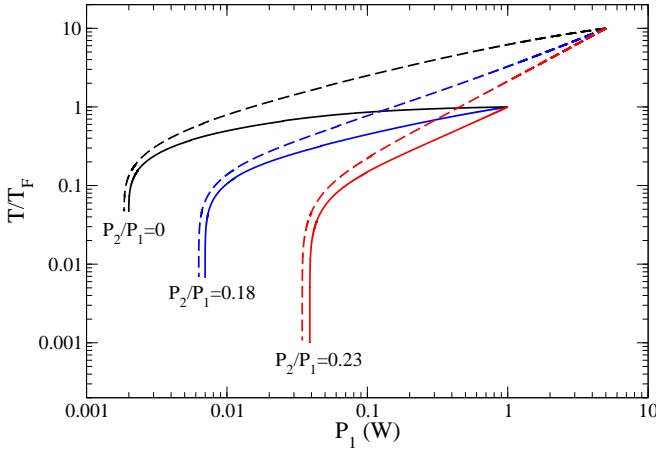


FIG. 2: (Color online) Dependence of the degeneracy factor $T=T_F$ upon the coning laser power P_1 during sympathetic forced evaporative cooling as determined by Eq. (6). The system is a mixture with N_f atoms of ^6Li and N_b atoms of ^{87}Rb trapped in a bichromatic optical dipole trap shaped by two lasers of power P_1 and P_2 at the wavelengths of $\lambda_1 = 1064\text{ nm}$ and $\lambda_2 = 740\text{ nm}$ for the $^6\text{Li}-^{87}\text{Rb}$ mixture as chosen in [35]. Two sets of curves are shown for different initial conditions and for different values of the ratio $P_2=P_1$, kept constant during the evaporation. The fermion-to-boson trapping frequency ratio, determined by $P_2=P_1$, is $\omega_f=\omega_b = 2.443$ for $P_2=P_1 = 0$, $\omega_f=\omega_b = 8.186$ for $P_2=P_1 = 0.18$ and $\omega_f=\omega_b = 15.911$ for $P_2=P_1 = 0.23$. For the same $P_2=P_1$ values, the other constant $U_b P_1^{-1/2} = k_B T_F$ which appears in Eq. (6) amounts to 18.73, 3.70 and 0.59, respectively. For simplicity, we set $\omega = 0$. We assume $N_f = 10^4$ is constant during the evaporation and, for the continuous (dashed) curves the initial number of bosons is $N_b = 2 \cdot 10^7$ ($N_b = 2 \cdot 10^9$), Fermi degeneracy $T=T_F = 1$ ($T=T_F = 10$) and $P_1 = 1\text{ W}$ ($P_1 = 5\text{ W}$). The minimum achievable $T=T_F$, corresponding mathematically to a singularity of Eq. (6) and physically to a fermion-boson heat capacity equality, (a) does not depend on N_f and N_b , provided that N_b is sufficiently large and (b) depends only slightly on the initial conditions for $T=T_F$ and P_1 , but (c) decreases appreciably if the trapping frequency ratio $\omega_f=\omega_b$ is increased.

is defined by the condition

$$(U_b + k_B T) \frac{\partial N_b^{\text{ex}}}{\partial T} - \frac{\partial E_b}{\partial T} - \frac{\partial E_f}{\partial T} = 0 : \quad (9)$$

For $U_b \ll k_B T$, a condition well satisfied at the singular point, we have

$$\frac{\partial N_b^{\text{ex}}}{\partial T} = \frac{1}{k_B T} \frac{\partial E_b}{\partial T} \frac{6}{24} \quad (3) \quad (4) , \quad (10)$$

therefore Eq. (9) is equivalent to

$$0.28 \frac{U_b}{k_B T} - 1 - C_b - C_f ; \quad (11)$$

where $C_s = \partial E_s / \partial T$ with $s = b, f$.

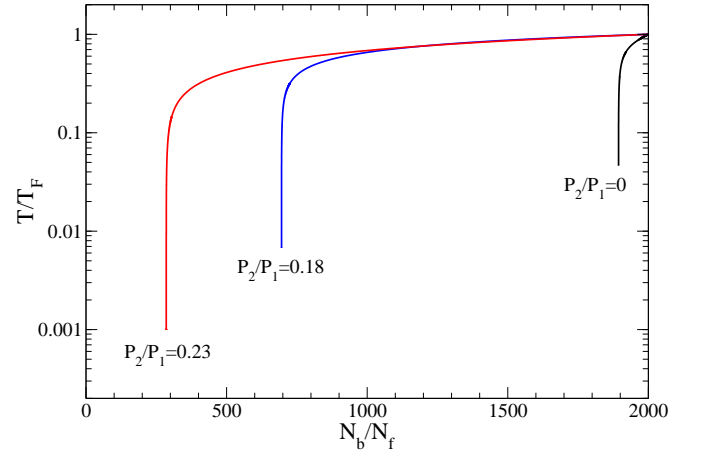


FIG. 3: (Color online) Dependence of the degeneracy factor $T=T_F$ upon the number of bosons (normalized to the number of fermions) during a sympathetic forced evaporative cooling driven by the laser power P_1 as determined by Eq. (6). The parameters are the same as in the case of the continuous curves in Fig. 2, with the initial values of $N_b = 2 \cdot 10^7$, $T=T_F = 1$, and $P_1 = 1\text{ W}$. It is evident that the use of larger $\omega_f=\omega_b$ ratios allows us to reach a deeper Fermi degenerate regime, which amounts to a gain by almost two orders of magnitude difference in the case of the larger $\omega_f=\omega_b$ ratio.

The sharp drop observed in $T=T_F$ before the singular point deserves some comments. At temperatures sufficiently low with respect to T_F and T_c , the energy of the mixture $E_b + E_f$ is dominated by the zero temperature Fermi energy $E_f(N_f; 0)$, see Appendix A. In this case, the right-hand side of the energy balance equation (2) can be approximated by $(\partial E_f(N_f; 0) / \partial N_f) dN_f$, and in the proximity of the singular point (i.e. at low temperatures), following Eq. (11) the left-hand side of the same balance can be written as $(C_b - C_f) dT$, where $C_s = \partial E_s / \partial T$ with $s = b, f$. The approximated energy balance thus gives

$$dT \sim \frac{dN_f}{N_f} \frac{\frac{3}{4} N_f k_B T_F}{C_b - C_f} ; \quad (12)$$

From Eq. (12) we see that a small decrease of the fermion trapping frequency induces a temperature decrease, the size of which depends on the value of $N_f k_B T_F = (C_b - C_f)$. Note that the denominator of this ratio contains a difference, not a sum, of the boson and fermion specific heats. The divergence of the derivative $dT = dN_f$ predicted at the critical point is certainly unphysical: we expect that a long time is needed to re-equilibrate the system in a freezing step $T \rightarrow T + dT$ with dT large. In this case, dissipative phenomena should be taken into account by a more complicated model in which the singular point will be substituted by a minimum. However, this does not change the meaning of the lowest reachable $T=T_F$ which is the point where fermion and boson specific heats do match.

In Fig. 3 we plot the dependence of $T=T_F$ upon the

number of bosons, normalized to the fermion number (assumed to be constant during the evaporation process). It is manifest that deeper Fermi degeneracy factors are obtained for higher trapping frequency ratios. This plot has to be compared to the one presented in Fig. 2 of [32] in which $T=T_F$ was shown versus a similar quantity (in our notation $(N_b^{(0)} - N_b)/N_f$ where $N_b^{(0)}$ is the number of initial bosons prior to evaporation). While our analysis confirms that the initial decrease in $T=T_F$ is faster for lower $\lambda_f=\lambda_b$ ratios, thus suggesting more efficient cooling – if measured by the drop in $T=T_F$ per unit of boson removed in the evaporation process – we also notice that the evaporation process extends much further for larger $\lambda_f=\lambda_b$ and allows to reach deeper Fermi degeneracy factors before stopping. Therefore, if the goal of the cooling process is the achievement of the lowest $T=T_F$ degeneracy parameters rather than saving bosons during the evaporative process [54], the use of larger $\lambda_f=\lambda_b$ is beneficial, at variance with [32].

The main issue in [32] is that no temporal dependence for the trapping frequencies was assumed (unlike in Eqns. (3-5)), which is unphysical for any realistic evaporative cooling strategy involving species-selective trapping strengths. The discussion in [32] also struggles with issues arising from more practical limitations, as commented in [41], in particular the fact that all the Fermi-Bose species available in practice will be affected by issues of spatial overlap in usual confining potentials, due to the smaller mass of the Fermi species (apart from the never considered $^{40}\text{K}-^{23}\text{Na}$ mixture). Also, for $\lambda_b=\lambda_f > 1$ the superfluid critical velocity of the Bose gas will become larger than the Fermi velocity, inhibiting scattering between fermions and bosons and then sympathetic cooling [55, 56]. Finally, a weaker trapping frequency for the Fermi species corresponds to a lower potential energy depth with respect to that of the bosons, resulting in significant fermion losses during the forced evaporative process of the bosons. As we discuss in the following, a large $\lambda_f=\lambda_b$ ratio is also beneficial in terms of improving the spatial overlap between fermions and bosons and therefore the cooling efficiency.

C. Spatial overlap between the fermion and the thermal Bose atoms

An even more realistic analysis of the cooling dynamics must also account for the intrinsic inhomogeneous character of the trapping potential as this will result in incomplete overlap between the Fermi and the Bose gases and consequently a decreased cooling efficiency. As introduced in [41], we express the spatial overlap i_j between two clouds of densities n_i and n_j , as

$$i_j = \frac{\int n_i n_j}{\int n_i \int n_j} = \frac{\int n_i^{1/2} n_j^{1/2} (r) d^3r}{\int n_i^{1/2} (r) d^3r \int n_j^{1/2} (r) d^3r}; \quad (13)$$

where i, j refer to the fermion (F), Bose condensate (B) or thermal boson (T) density profiles. The fraction of

atoms that share the same region of space is thus given by $\frac{2}{i_j}$. The Bose atoms available for cooling are those having a non-zero specific heat, i.e. those in a thermal state. Finite overlap between the thermal bosons and the Fermi atoms will result in a decrease in the cooling rate with respect to the case of ideal overlap. An accurate evaluation of the cooling rate should take into account kinetic equations for the two interacting gases. In a pessimistic, conservative fashion, we can assume that the cooling rate q is decreased by a factor equal to the fraction of atoms that can actually exchange energy without any mass transport involved, as $q_{\text{cool}} \propto \frac{2}{F_T} q_{\text{cool}}$. The minimum attainable degeneracy parameter $T=T_F$ correspondingly increases as $T=T_F \propto \frac{2}{F_T} T=T_F$. This static estimate does not take into account the timescale over which fermions and bosons exchange energy through elastic collisions, and the particle relocation along the trap volume, but it can be considered as an upper limit to the effect of partial overlap. This analysis requires the density profiles of the condensate and the non-condensed thermal boson to be computed independently, following the discussion of a Fermi-Bose mixture at finite temperature reported in [57].

The dependence of the spatial overlap parameters F_B and F_T on temperature, boson number, and trapping frequency ratio is shown in Fig. 4. As the temperature drops below T_c a finite condensate fraction appears; the fermion-thermal boson overlap starts to decrease, and the fermion-condensate overlap increases. There is a limit to F_B for a given $\lambda_f=\lambda_b$, however, since the cloud of less massive fermions will have a much larger spatial radius and thus a strong relative confinement is required to improve the fermion-Bose condensate overlap. The overlap dependence on number ratio is rather straightforward, with a gradual decrease in fermion-condensate overlap as bosons are evaporated and an almost flat behaviour for F_T since N_b^{ex} is roughly constant for a given temperature and boson losses manifest as a decrease in the condensate fraction and have a minimal effect on the thermal cloud.

The effect of the spatial overlap on the minimum reachable Fermi degeneracy factor $T=T_F$ is depicted in Fig. 5, with the choice of interspecies scattering length of the Li-Rb system corresponding to the pessimistic scenario of repulsive interaction (see [58] for the issues related to its measurement). It is evident that about one order of magnitude may be lost in the achievable minimum degeneracy factor when the overlap factor is taken into account, although we conjecture that with a full kinetic analysis the actual result will be located in between the two curves. The situation is analyzed in more detail in Fig. 6, which shows F_T versus $\lambda_f=\lambda_b$ and $T=T_c$. During the cooling process, i.e. as $T=T_c$ decreases, the optimal overlap is shifted to larger values of $\lambda_f=\lambda_b$, until the minimum of the Fermi degeneracy is reached as shown in the contour plot of Fig. 7. This suggests the use of a time-variable trapping strategy, initial with lower values of $\lambda_f=\lambda_b$, then increased in time by increasing the power ratio $P_2=P_1$. Such a time-dependent relative con-

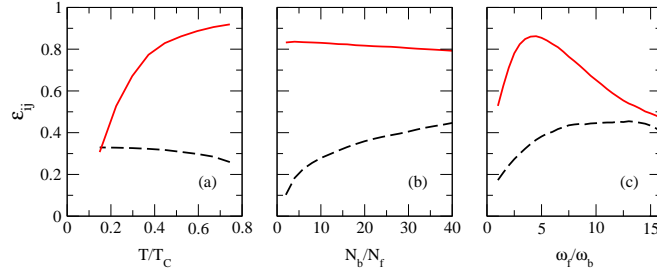


FIG. 4: (Color online) Overlap parameters e_{FB} (dashed line) and e_{FT} (solid line) versus (a) T/T_C , (b) N_b/N_f , and (c) ω_f/ω_b . Plots made with other two parameters held at given values of $N_b/N_f = 15$, $T/T_C = 0.3$, $\omega_f/\omega_b = 3$, in the case of a scattering length for Rb of $a_{bb} = +5.8$ nm and an interspecies scattering length $a_{fb} = +0.5$ nm (with the same values also used for the plots in Figs. 5-7).

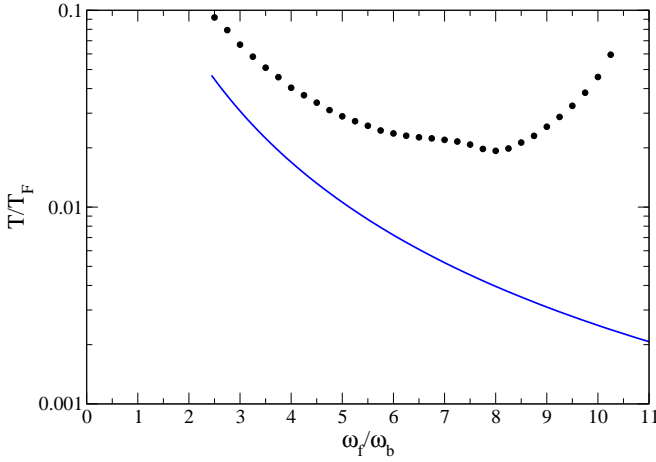


FIG. 5: (Color online) Plots of the minimum $T=T_F$ reached during the evaporative cooling process in an optical dipole trap, without (line) and with (dots) the fermion-atom spatial overlap taken into account. The curve and dots start at the lowest possible value of $\omega_f/\omega_b = 2.443$, which is the 'natural' trapping frequency ratio for a $^6\text{Li}-^87\text{Rb}$ mixture with the deconing laser beam switched on ($P_2 = 0$).

nement strategy is not the only way to optimize the Fermi degeneracy factor, however. In the following, we will discuss a similar procedure which exploits the advantages of reducing the dimensionality of the system when Fermi degeneracy is approached.

III. HEAT CAPACITY MATCHING THROUGH LOWER DIMENSIONALITY

As an alternative to the cooling strategy described above, we discuss here the possibility to match the heat capacity of Bose and Fermi gases at the lowest possible $T=T_F$ by exploiting lower dimensionality traps. Ultimately, the matching between the specific heats of Bose and Fermi degenerate gases depend on the scaling of the heat capacities with temperature, and this in turn depends upon the dimensionality of the Bose gas. As

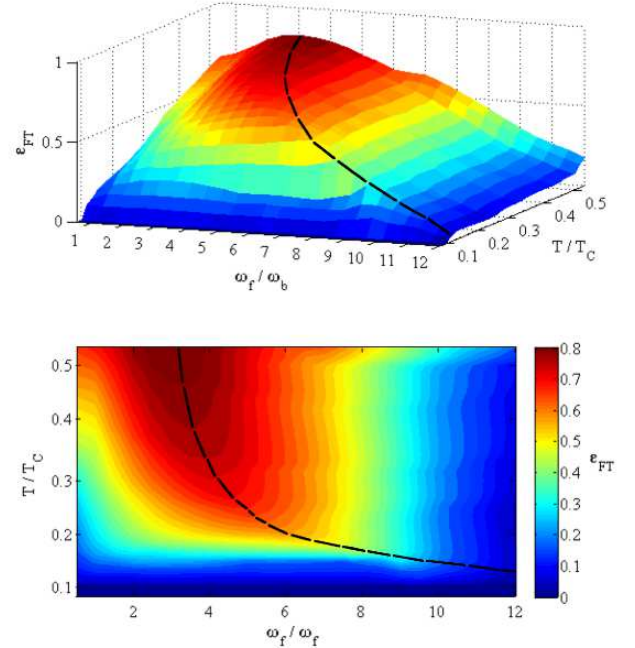


FIG. 6: (Color online) Three-dimensional plot and two-dimensional contour plot of the e_{FT} dependence on ω_f/ω_b , and T/T_C . Significant overlap values for trapping ratios in the range of $\omega_f/\omega_b \sim 3-7$ are evident at relatively large temperature ratios T/T_C . At lower temperatures, the optimal overlap is achieved at higher trapping frequencies ratios. The optimal path maximizing the overlap is highlighted by the dashed line in both plots.

discussed in [59, 60] and demonstrated in [61, 62], a dramatic increase in the trapping frequency in one (or two) trapping axes will result in an effective two- (or one-) dimensional system. This in turn allows for a better matching of the heat capacities since the Bose gas dependence on temperature will become milder than in the full 3D case. In order to gain quantitative insights on how to realize such a matching, we first consider noninteracting gases in a harmonic potential, with the number N_{fb} of particles fixed.

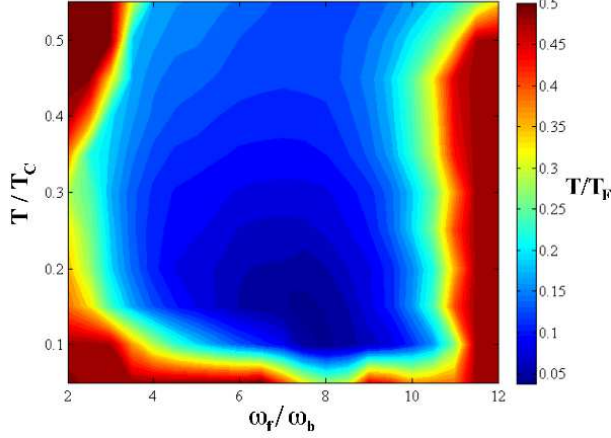


FIG. 7: (Color online) Contour plot of the Fermi degeneracy factor T/T_F versus the Bose degeneracy factor T/T_c and the trapping frequency ratio ω_f/ω_b . The lower Fermi degeneracy factor of $T/T_F \approx 0.02$ is obtained for $\omega_f/\omega_b \approx 8$.

The total number of fermions and bosons is evaluated as (+ for fermions, - for bosons):

$$N_{f,b}(\pm; T) = \sum_{j=0}^{\infty} \frac{g_j}{e^{(E_j \pm \mu)/k_B T} \pm 1}, \quad (14)$$

where g_j is the degeneracy of energy level E_j , the chemical potential, k_B Boltzmann constant, and T the temperature, with the number of particles $N_{f,b}$ fixed. Solving this equation numerically for $\mu = \mu(T)$, we can then calculate the total energy

$$E_{f,b}(T) = \sum_{j=0}^{\infty} \frac{g_j E_j}{e^{(E_j \pm \mu)/k_B T} \pm 1}, \quad (15)$$

and from this we obtain the heat capacity as $C(T) = \partial E / \partial T$. In the calculation below, we assign $N_{f,b} = 10^4$, and assume the initial trap to be isotropic with the trapping frequency $\omega = 2 \times 15.87$ kHz. The numerical calculations for 2D and 3D are straightforward, while for 1D some approximations are necessary to reduce the simulation time to realistic values.

A. 2D and 3D traps

For atoms trapped in a three dimensional harmonic potential $V(r) = \frac{1}{2} m \omega^2 r^2$, the energy eigenvalues E_j ($j=0,1,2,\dots$) are given by $E_j^{3D} = (j+3/2)\hbar\omega$. Since the trap is three-dimensional and isotropic, the degeneracy g_j of the energy levels is given by $g_j = (j+1)(j+2)/2$. The number of particles for bosons (-) and fermions (+) is:

$$N_{f,b}^{3D} = \frac{1}{2} \sum_{j=0}^{\infty} \frac{(j+1)(j+2)}{e^{((j+3/2)\hbar\omega \pm \mu)/k_B T} \pm 1}, \quad (16)$$

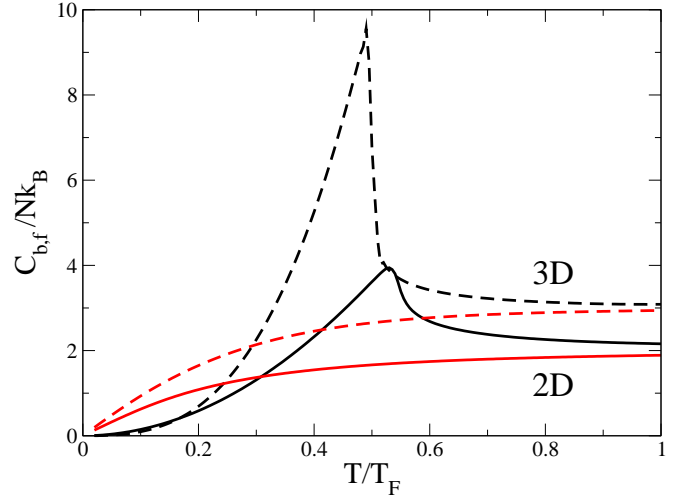


FIG. 8: (Color online) Heat capacity curves of bosons and fermions in 3D (dashed curves) and 2D (solid curves) in an isotropic harmonic trap, with the bosons exhibiting non-monotonic behaviour. The crossing point between the Bose and Fermi curves for the 2D case occurs at a slightly higher T/T_F value, ruling out its use for a more favourable cooling of fermions.

The upper limit Q in the summation should be infinity in principle, but a value of $Q = 1500$ is sufficient for numerical convergence. For the given parameters $N_{f,b}$ and ω we solve the above two equations at different temperatures, and then calculate the heat capacities. As depicted in Fig. 8, the Bose and Fermi heat capacities intersect each other at $T \approx 0.293 T_F$, with the three-dimensional Fermi temperature $T_F^{3D} = (6N_f)^{1/3} \hbar\omega/k_B$. The situation is very similar for atoms trapped in a 2D isotropic harmonic potential, except that now the energy eigenvalues are given by $E_j^{2D} = (j+1)\hbar\omega$, with degeneracy $g_j = j+1$, and Q needs to be increased to 10^6 to achieve adequate convergence. The two heat capacities curves intersect each other at $T \approx 0.308 T_F$ where the 2D Fermi temperature T_F is given by $T_F^{2D} = (2N_f)^{1/2} \hbar\omega/k_B$. From Fig. 8 we see that going from a full 3D to a 2D system actually slightly worsens the heat capacity matching, yielding a higher T/T_F at the point where C_b and C_f intersect each other. However, further reduction to a 1D system results in complete matching of the heat capacities, as we will see below.

B. 1D trap

For atoms in a 1D trap, the energy eigenvalues are given by $E_j^{1D} = (j+1/2)\hbar\omega$, with degeneracy $g_j = 1$. If we follow the same steps as the 2D and 3D cases, the upper summation limit Q (see Eq. (16)) must be extremely large in order to reach convergence and approximations are required for the one-dimensional trap analysis. These approximations are outlined in Appendix B

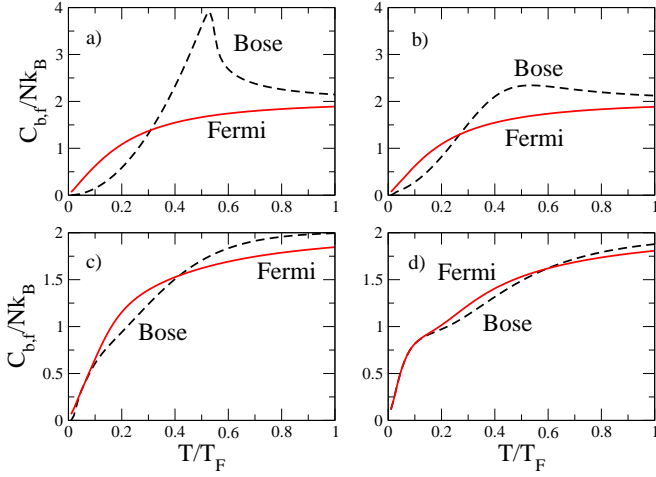


FIG. 9: (Color online) Heat capacity curves of bosons (black, dashed) and fermions (red, continuous). We consider for simplicity the case of equal number of bosons and fermions $N_b = N_f = 10^4$ with equal mass $m_b = m_f$. Curves in plots (a), (b), (c) and (d) are in 2D traps with $k = \omega_y/\omega_x$ equals to 1, 2.5, 10^3 , 2 and $5 \cdot 10^4$ respectively, with the case in (d) showing an initial plateau of the heat capacities at $T/T_F \ll 1$ before reaching the high temperature limit of a 2D gas.

and with them we obtain the Fermi and Bose energies, from which the heat capacities are evaluated. To take full advantage of the gain in the heat capacity matching in 1D traps it is helpful to investigate how heat capacities of bosons and fermions change when we gradually reduce the dimension of the trap. We assume that the atoms are first trapped in a 2D trap with trapping frequencies along the two dimensions ω_y and ω_x , and then this relative confinement parameter k is gradually increased from 1 to infinity. The system will be effectively 1D when $k_B T \ll \hbar \omega_x$. We evaluate the heat capacities of bosons and fermions at different values of k . The results are shown in Fig. 9 (a-d). As k increases, the shape of the heat capacity curve of bosons becomes more similar to that of fermions, in the sense that it slowly loses the peak structure and the curvature near zero temperature begins to resemble that of fermions. If k is further increased (case (c)) there will be a region where the two curves completely coincide with each other. This is consistent with the previous result we obtained for an ideal 1D trap. In Fig. 9 (d) the heat capacity curves of bosons and fermions are shown at an even higher aspect ratio, to emphasize the crossover from the 1D case to the 2D case at high temperatures. In the ideal 1D case, the heat capacity curves are identical, as simply explained in the canonical ensemble approach [63, 64]. Indeed, the total internal energy of fermions in a 1D harmonic trap only differs from that of the bosons by the Fermi zero-point energy $E_0 = N_f(N_f + 1)\hbar\omega_x/2$, and therefore the two systems have identical heat capacities.

The existence of this crossover indicates that we can control the heat capacity matching of bosons and

fermions by changing the ratio of the two trapping frequencies in a 2D trap. Thus one possible solution to improve the cooling efficiency is to first evaporate in a 3D trap and then, when the Fermi degeneracy starts to reach about $T/T_F \approx 0.3$, to increase the trapping frequencies achieving a quasi-one dimensional system, then continuing the evaporation process. A possible limitation of this technique comes from the larger collisional loss rate as a result of the increased confinement. Also, as studied for achieving Bose condensation of hydrogen atoms, the nearly 1D character of the evaporative cooling [65] may lead to non-ergodic evaporation limiting its efficiency [66], although this has not prevented achievement of Bose degeneracy [67].

IV. CONCLUSIONS

We have examined the thermodynamics of evaporative and sympathetic cooling in a Fermi-Bose mixture, and identified possible ways to achieve a lower Fermi degeneracy factor T/T_F . Thermodynamical considerations are based on general assumptions and measurable, phenomenological inputs, like heating rate and specific heat, and provide a solid framework to discuss cooling dynamics regardless of sophisticated microscopic models [68]. They also allow for comparison with experimental results, such as those discussed in [69, 70, 71, 72, 73, 74], or for the inclusion of more realistic inputs such as the specific heat of an interacting gas [75]. Although we have focused the attention on the particular ^6Li - ^{87}Rb mixture, the extension to other Fermi-Bose combinations is straightforward, furthermore benefiting from more favourable interspecies thermalization properties with respect to this particular mixture, for which limitations in elastic scattering and use of Feshbach resonances have been experimentally evidenced [43, 76].

Among the main results we have obtained, we have discussed two different cooling strategies: constructing a species-selective trap with independently tunable Fermi and Bose trapping frequencies, and creating traps with reduced dimensionality in the latest stage of evaporation. We have shown that different trapping ratios lead to distinctly different cooling trajectories. However, incomplete spatial overlap will not only result in a longer cooling time needed to attain a given temperature, but will also increase the temperature at which the heating rate will balance the cooling rate. When the progressive depletion of the bosonic thermal cloud is taken into account, optimized cooling requires time-dependent trapping strengths. Additionally, we have discussed how to exploit the strong dependence of the bosonic specific heat upon dimensionality to create nearly one-dimensional traps in the ultimate stage of sympathetic cooling. This will be of particular relevance for various planned studies of Fermi gases in optical lattices [77] in which bichromatic optical traps are not viable.

APPENDIX A : BOSE AND FERMION GASES IN A 3D HARMONIC TRAP OF FINITE DEPTH

We report here the expressions for the energy and the number of particles of ideal degenerate Bose and Fermi gases confined in a three-dimensional harmonic trap of finite depth.

For the trapped bosons we start with the exact expressions of the energy and of the number of particles in a general 3D harmonic potential:

$$E_b = \sum_{n_x=0}^{\infty} \sum_{n_y=0}^{\infty} \sum_{n_z=0}^{\infty} \frac{E_{n_x, n_y, n_z}}{e^{(E_{n_x, n_y, n_z})/k_B T}}; \quad (A1)$$

$$N_b = \sum_{n_x=0}^{\infty} \sum_{n_y=0}^{\infty} \sum_{n_z=0}^{\infty} \frac{1}{e^{(E_{n_x, n_y, n_z})/k_B T}}; \quad (A2)$$

where $E_{n_x, n_y, n_z} = \hbar \omega_x (n_x + 1/2) + \hbar \omega_y (n_y + 1/2) + \hbar \omega_z (n_z + 1/2)$. As usual, we write $N_b = N_b^0 + N_b^{\text{ex}}$, where $N_b^0 = (e^{E_{0,0,0}/k_B T} - 1)^{-1}$ is the number of bosons in the ground state and N_b^{ex} the number of those thermally excited. In order that the number of particles remains positive, it is necessary for the chemical potential to satisfy $(\mu) \leq E_{0,0,0}$. At temperatures $T \leq T_c$, where T_c is the Bose-Einstein condensation critical temperature, the chemical potential is frozen to its maximum value. In general, (μ) and all the other thermodynamic quantities can be evaluated explicitly as a power series expansion in the two parameters $(\mu) \leq E_{0,0,0}$ and $\hbar \omega_b/k_B T$, where $\omega_b = (\omega_x^2 + \omega_y^2 + \omega_z^2)^{1/2}$ [78]. In the case $T \leq T_c$ and $\hbar \omega_b \ll k_B T$, which is relevant to the experimental situations discussed here, we can restrict to the lowest order and write

$$E_b = 3 (4) \frac{(k_B T)^4}{(\hbar \omega_b)^3}; \quad (A3)$$

$$N_b^{\text{ex}} = (3) \frac{k_B T}{\hbar \omega_b}; \quad (A4)$$

where ζ is the Riemann zeta function. Alternatively, the above two results can be obtained using the semiclassical density of states

$$\rho_b(E) = \frac{d}{dE} \frac{\frac{1}{6} E^3}{\hbar \omega_x \hbar \omega_y \hbar \omega_z} = \frac{E^2}{2 (\hbar \omega_b)^3} \quad (A5)$$

and the continuum approximation

$$E_b = \int_0^{\infty} \frac{E}{e^{E/k_B T} - 1} \rho_b(E) dE; \quad (A6)$$

$$N_b^{\text{ex}} = \int_0^{\infty} \frac{1}{e^{E/k_B T} - 1} \rho_b(E) dE; \quad (A7)$$

For a trap of finite depth schematized as a harmonic potential truncated at energy U_b , we thus write

$$E_b = \int_0^{U_b} \frac{E}{e^{E/k_B T} - 1} \rho_b(E) dE = \frac{(k_B T)^4}{(\hbar \omega_b)^3} \frac{1}{2} \int_0^{\frac{U_b}{k_B T}} \frac{t^3}{e^t - 1} dt; \quad (A8)$$

$$N_b^{\text{ex}} = \int_0^{U_b} \frac{1}{e^{E/k_B T} - 1} \rho_b(E) dE = \frac{(k_B T)^3}{(\hbar \omega_b)^3} \frac{1}{2} \int_0^{\frac{U_b}{k_B T}} \frac{t^2}{e^t - 1} dt; \quad (A9)$$

Consider now a system of N_f fermions confined by a harmonic trap having characteristic frequencies $\hbar \omega_x, \hbar \omega_y, \hbar \omega_z$. Under the condition $\hbar \omega_x, \hbar \omega_y, \hbar \omega_z \ll k_B T$, a continuum approximation holds as in the boson case, so that the fermion counterparts of Eqs. (A1) and (A2) can be simplified to

$$E_f = \int_0^{\infty} \frac{E}{e^{(E-\mu)/k_B T} + 1} \rho_f(E) dE; \quad (A10)$$

$$N_f = \int_0^{\infty} \frac{1}{e^{(E-\mu)/k_B T} + 1} \rho_f(E) dE; \quad (A11)$$

where $\rho_f(E) = E^2/2 (\hbar \omega_f)^3$ and $\omega_f = (\omega_x^2 + \omega_y^2 + \omega_z^2)^{1/2}$. Note that in the above expressions we have neglected the zero-point energy which is justified since for fermions

$E_{0,0,0} \ll k_B T$. The accuracy of the continuum approximation introduced above is discussed in detail in [79]. The chemical potential (μ) can be eliminated between Eqs. (A10) and (A11) by means of the standard Sommerfeld expansion in powers of temperature. By keeping terms only to second order in T , we have the well known result

$$E_f(N_f; T) = E_f(N_f; 0) + \frac{\pi^2}{6} (k_B T)^2 \rho_f(E_F); \quad (A12)$$

where the Fermi energy E_F is related to N_f by

$$N_f = \int_0^{E_F} \rho_f(E) dE = \frac{1}{6} \frac{E_F^3}{\hbar \omega_f}; \quad (A13)$$

and the zero temperature term $E_f(N_f; 0)$ is given by

$$E_f(N_f; 0) = \int_0^{E_F} E \rho_f(E) dE = \frac{E_F^4}{8 (\hbar \omega_f)^3}; \quad (A14)$$

Making use of the relationship between the Fermi energy and the number of fermions, we finally obtain

$$E_f = \frac{3}{4} \pi^2 N_f^4 \hbar \omega_f + \frac{\pi^2}{2} \pi^2 N_f^2 \frac{(k_B T)^2}{\hbar \omega_f}; \quad (A15)$$

Equations (A13) and (A15) are valid also for fermions trapped into a harmonic potential truncated at energy U_f , provided that $U_f \gg E_F, k_B T$.

APPENDIX B: INTERNAL ENERGY FOR A 1D TRAPPED IDEAL FERMIGAS

The total atom numbers in one dimension N_b^{1D} and N_f^{1D} are given by Eq. (14), with $g_j = 1$. However, the upper summation limit Q (see Eqs. (16)) needed for convergence becomes unreasonably large in one dimension [80], and thus approximations are required.

For fermions, we can directly replace the summation with an integral in the case of $k_B T \gg \epsilon$:

$$N_f^{1D} = \sum_{j=0}^{\infty} \frac{1}{e^{((j+1/2)\pi\epsilon/k_B T) + 1}} \quad (B1)$$

Similarly, the total energy is given by

$$E_f = \sum_{j=0}^{\infty} \frac{1}{e^{((j+1/2)\pi\epsilon/k_B T) + 1}} \quad (B2)$$

The total number of bosons is given by

$$N_b^{1D} = \sum_{j=0}^{\infty} \frac{1}{e^{((j+1/2)\pi\epsilon/k_B T) + 1}} \quad (B3)$$

The second summation term can be evaluated by integral using the Euler-Maclaurin formula:

$$F(x) = \int_a^b F(x) dx + \frac{F(a) + F(b)}{2} + \sum_{k=1}^{\infty} \frac{B_{2k}}{(2k)!} [F^{(2k-1)}(b) - F^{(2k-1)}(a)] + R$$

where $B_2 = 1/6$, $B_4 = -1/30, \dots$ are the Bernoulli numbers, and R is the remainder term. In the case of $k_B T \gg \epsilon$, the first term ($k = 1$) in the expansion is sufficient, giving:

$$N_b^{1D} = \frac{1}{e^{((1/2)\pi\epsilon/k_B T) + 1}} + \frac{1}{2} \frac{1}{e^{((3/2)\pi\epsilon/k_B T) + 1}} + \frac{1}{12K_B T} \frac{1}{e^{((3/2)\pi\epsilon/k_B T) + 1}} \quad (B4)$$

Having fixed N , we solve this equation numerically for at different temperatures to obtain $\epsilon = \epsilon(T)$, and then apply the Euler-Maclaurin formula again to obtain the total energy E_b^{1D} .

The discussion above holds for a one dimensional Bose gas. In the case of a trapping frequency range for which there is a smooth crossover from two dimensions to one dimension, we recall that the number of particles in a 2D trap is given by:

$$N_{f;b}^{2D} = \sum_{i,j=0}^{\infty} \frac{1}{e^{[(i+1/2)\pi\epsilon_1 + (j+1/2)\pi\epsilon_2]/k_B T + 1}} \quad (B5)$$

Running two independent indexes is computationally very inefficient and slow. We therefore assume $\epsilon_1 = \epsilon$ and $\epsilon_2 = k\epsilon$ where k is a positive integer. The summation is run until $(i+kj) = Q$ which, with Q large enough, yields a good approximation. Now $N_{f;b}^{2D}$ becomes:

$$N_{2d} = \sum_{i,j=0}^{i+kj=Q} \frac{1}{e^{[(i+kj)\pi\epsilon + (1/2 + k/2)\pi\epsilon]/k_B T + 1}} \quad (B6)$$

where $\text{floor}(j/k)$ is the nearest integer less than or equal to j/k . In this way only one index is present, allowing to improve significantly the computational speed.

ACKNOWLEDGMENTS

MBH and QW acknowledge support from the Dartmouth Graduate Fellowship program, and MBH also acknowledges support from the Gordon Hull and NSF-GAANN fellowships. CP and RO acknowledge partial support through Conanziamento MUR protocols 2002027798-001, and RO also acknowledge partial support by the NSF through the Institute for Theoretical Atomic and Molecular Physics at Harvard University and the Smithsonian Astrophysical Observatory.

-
- [1] A. L. Fetter and A. A. Svidzinsky, *J. Phys. Condens. Matter* **13**, R135 (2001); A. J. Leggett, *Rev. Mod. Phys.* **73**, 307 (2001); C. J. Pethick and H. Smith, *Bose-Einstein condensation in dilute gases* (Cambridge University Press, Cambridge, 2002); L. P. Pitaevskii and S. Stringari, *Bose-Einstein condensation*, (Oxford Science Publications, Oxford, 2003).
- [2] Q. Chen, J. Stajic, S. Tan, and K. Levin, *Phys. Rep.* **412**, 1 (2005).
- [3] B. DeMarco and D. S. Jin, *Science* **291**, 2570 (1999).
- [4] M. W. Zwierlein et al., *Science* **435**, 1047 (2005).
- [5] D. E. M. Iller et al., *Phys. Rev. Lett.* **99**, 070402 (2007).
- [6] M. Crescimanno, C. G. Kaoy, and R. Peterson, *Phys. Rev. A* **61**, 053602 (2000).
- [7] M. J. Holland, B. DeMarco, and D. S. Jin, *Phys. Rev. A* **61**, 053610 (2000).
- [8] Z. Hadzibabic et al., *Phys. Rev. Lett.* **91**, 160401 (2003).
- [9] M. Bartenstein et al., *Phys. Rev. Lett.* **92**, 120401 (2004).
- [10] M. Zwierlein, A. Schirotzek, C. H. Schunck, and W. Ketterle, *Science* **311**, 492 (2006).
- [11] G. B. Partridge, W. Li, R. I. Kamar, Y. Liao, and R. Hulet, *Science* **311**, 503 (2006).
- [12] M. Zwierlein, A. Schirotzek, C. H. Schunck, and W. Ketterle, *Nature* **442**, 54 (2006).
- [13] Y. Shin, M. W. Zwierlein, C. H. Schunck, A. Schirotzek, and W. Ketterle, *Phys. Rev. Lett.* **97**, 030401 (2006).
- [14] K. Gunter, T. Stoferle, H. Moritz, M. Kohl, and T. Esslinger, *Phys. Rev. Lett.* **96**, 180402 (2006).
- [15] S. Ospelkaus et al., *Phys. Rev. Lett.* **96**, 180403 (2006).
- [16] Q. Chen, C. A. Regal, M. Greiner, D. S. Jin, K. Levin, *Phys. Rev. A* **73**, 041601(R) (2006).
- [17] A. Bulgac, J. E. D. Nut, and P. Magierski, *Phys. Rev. Lett.* **96**, 090404 (2006).
- [18] C.-C. Chien, Q. Chen, Y. He, and K. Levin, *Phys. Rev. Lett.* **97**, 090402 (2006).
- [19] H. F. Hess, *Phys. Rev. B* **34**, 3476 (1986).
- [20] O. J. Luiten, M. W. Reynolds, and J. T. M. Walraven, *Phys. Rev. A* **53**, 381 (1996).
- [21] M. Holland, J. Williams, and J. Cooper, *Phys. Rev. A* **55**, 3670 (1997).
- [22] O. H. Pakarinen and K. A. Suominen, *Phys. Rev. A* **62**, 025402 (2000).
- [23] H. Wu, E. Arimondo, and C. J. Foot, *Phys. Rev. A* **56**, 560 (1997).
- [24] E. Carboneschi, C. Menchini, and E. Arimondo, *Phys. Rev. A* **62**, 013606 (2000).
- [25] A. V. Avidenkov, *J. Phys. B* **37**, 237 (2004).
- [26] M. K. Olsen, L. I. Plimak, V. I. Kruglov, and J. J. Hope, *Laser Physics* **12**, 21 (2002).
- [27] M. Yamashita, M. Koashi, and N. Imoto, *Phys. Rev. A* **59**, 2243 (1999).
- [28] P. J. J. Tol, W. Hogervorst, and W. Vassen, *Phys. Rev. A* **70**, 013404 (2004).
- [29] D. Comparat, et al., *Phys. Rev. A* **73**, 043410 (2006).
- [30] D. A. Butts and D. S. Rokhsar, *Phys. Rev. A* **55**, 4346 (1997).
- [31] W. Geist, L. You, and T. A. B. Kennedy, *Phys. Rev. A* **59**, 1500 (1999).
- [32] L. D. Carr and Y. Castin, *Phys. Rev. A* **69**, 043611 (2004).
- [33] A. G. Truscott, K. E. Strecker, W. Im Alexander, G. B. Partridge, and R. G. Hulet, *Science* **291**, 2570 (2001).
- [34] C. Presilla and R. Onofrio, *Phys. Rev. Lett.* **90**, 030404 (2003).
- [35] R. Onofrio and C. Presilla, *J. Stat. Phys.* **115**, 57 (2004).
- [36] In the case of the ^6Li - ^{87}Rb mixture, there is no evidence that the Lithium atoms are thermalized at the measured temperature of the Rubidium gas, due to the slow thermalization between ^6Li and ^{87}Rb (Philippe Courteille, private communication).
- [37] J. M. McNamara, T. Jeltsov, A. S. Tychkov, W. Hogervorst, and W. Vassen, *Phys. Rev. Lett.* **97**, 080404 (2006).
- [38] F. Ferlaino, E. de Miranda, G. Roati, G. Modugno, and M. Inguscio, *Phys. Rev. Lett.* **92**, 140405 (2004).
- [39] F. Schreck et al., *Phys. Rev. Lett.* **87**, 080403 (2001).
- [40] J. Goldwin, S. Inouye, M. L. Olsen, B. Newman, B. D. DePaola, and D. S. Jin, *Phys. Rev. A* **70**, 021601(R) (2004).
- [41] M. A. Brown-Hayes and R. Onofrio, *Phys. Rev. A* **70**, 063614 (2004).
- [42] R. Côte, R. Onofrio, and E. Timmermans, *Phys. Rev. A* **72**, 041605(R) (2005).
- [43] C. Silber et al., *Phys. Rev. Lett.* **95**, 170408 (2005).
- [44] M. Brown-Hayes, Q. Wei, W.-J. Kim, and R. Onofrio, *Laser Physics* **17**, 514 (2007).
- [45] M. Taglieber, A. C. Voigt, T. Aoki, T. W. Hansch, and K. Dieckmann, *Phys. Rev. Lett.* **100**, 010401 (2008).
- [46] R. Gonzalez-Ferez, M. Mayle, and P. Schmelcher, *EPL* **78**, 53001 (2007).
- [47] M. Aymar and O. Dulieu, *J. Chem. Phys.* **122**, 204302 (2005).
- [48] K. M. O'Hara, M. E. Gehm, S. R. Granade, and J. E. Thomas, *Phys. Rev. A* **64**, 051403(R) (2001).
- [49] W. Ketterle and N. J. Van Druten, in *Advances in Atomic, Molecular, and Optical Physics*, edited by B. Bederson and H. Walthers (Academic Press, San Diego, 1996), Vol. 37, p. 181.
- [50] K. B. Davis, M. O. Mewes, and W. Ketterle, *Appl. Phys. B* **60**, 155 (1995).
- [51] M. Wouters, J. Tempere, and J. T. Devreese, *Phys. Rev. A* **66**, 043414 (2002).
- [52] R. Onofrio and C. Presilla, *Phys. Rev. Lett.* **89**, 100401 (2002).
- [53] There is a trade-off in decreasing the boson trapping frequency ω_b since the efficiency of evaporative cooling in itself is inversely proportional to the boson heat capacity. Also, a smaller ω_b implies lower densities of the Bose cloud, implying slower thermalization. Cooling strategies in which the boson trapping frequency is instead kept constant, while the fermion trapping frequency is increased, are possible alternatives to overcome these limitations.
- [54] It is worth to point out that in most of the experiments using Fermi-Bose mixtures and focusing on fermion studies, the residual Bose component is anyway removed after sympathetic cooling.
- [55] A. P. Chikkatur, A. Gorlitz, D. M. Stamper-Kurn, S. Inouye, S. Gupta, and W. Ketterle, *Phys. Rev. Lett.* **85**, 483 (2000).
- [56] E. Timmermans, *Phys. Rev. Lett.* **87**, 240403 (2001).
- [57] F. Dalfovo, S. Giorgini, L. Pitaevskii, and S. Stringari, *Rev. Mod. Phys.* **71**, 463 (1999).

- [58] C. Marzok, B. Deh, Ph. W. Courteille, and C. Zimmermann, *Phys. Rev. A* **76**, 052704 (2007).
- [59] J.J. Rehr and N.D. Mermin, *Phys. Rev. B* **1**, 3160 (1970).
- [60] V. Bagnato and D. Kleppner, *Phys. Rev. A* **44**, 7439 (1991).
- [61] W. Ketterle and N.J. van Druten, *Phys. Rev. A* **54**, 656 (1996).
- [62] H. Moritz, T. Stoferle, K. Guenter, M. Kohl, and T. Esslinger, *Phys. Rev. Lett.* **94**, 210401 (2005).
- [63] K. Schonhammer, *Am. J. Phys.* **68**, 1032 (2000).
- [64] W.J. Mullin and J.P. Fernandez, *Am. J. Phys.* **71**, 661 (2003).
- [65] P.W.H. Pinkse et al., *Phys. Rev. A* **57**, 4747 (1998).
- [66] E.L. Surkov, J.T.M. Walraven, and G.V. Shlyapnikov, *Phys. Rev. A* **53**, 3403 (1996).
- [67] A. Gorlitz et al., *Phys. Rev. Lett.* **87**, 130402 (2001); F. Schreck et al., *Phys. Rev. Lett.* **87**, 080403 (2001); M. Greiner, I. Bloch, O. Mandel, T.W. Hansch, and T. Esslinger, *Phys. Rev. Lett.* **87**, 160405 (2001); H. Moritz, T. Stoferle, M. Kohl, and T. Esslinger, *Phys. Rev. Lett.* **91**, 250402 (2003).
- [68] P.B. Blakie, E. Toth, and M.J. Davis, *J. Phys. B* **40**, 3273 (2007).
- [69] C. Raman et al., *J. Low Temp. Phys.* **122**, 99 (2001).
- [70] F. Gebier et al., *Phys. Rev. A* **70**, 013607 (2004).
- [71] J. Kinast et al., *Science* **307**, 1296 (2005).
- [72] R. Gati, B. Hemmerling, J. Fölling, M. Albiez, and M.K. Oberthaler, *Phys. Rev. Lett.* **96**, 130404 (2006).
- [73] R. Gati et al., *New J. Phys.* **8**, 189 (2006).
- [74] L. Luo, B. Clancy, J. Joseph, J. Kinast, and J.E. Thomas, *Phys. Rev. Lett.* **98**, 080402 (2007).
- [75] S. Giorgini, L.P. Pitaevskii, and S. Stringari, *J. Low Temp. Phys.* **109**, 309 (1997).
- [76] B. Deh, C. Marzok, C. Zimmermann, and Ph. W. Courteille, *Phys. Rev. A* **77**, 010701(R) (2008).
- [77] A. Albus, F. Illuminati, and J. Eisert, *Phys. Rev. A* **68**, 023606 (2003); F. Illuminati and A. Albus, *Phys. Rev. Lett.* **93**, 090406 (2004); M. Cramer, J. Eisert, and F. Illuminati, *Phys. Rev. Lett.* **93**, 190405 (2004); D.W. Wang, M.D. Lukin, and E. Demler, *Phys. Rev. A* **72**, 051604(R) (2005); M. Iskin and C.A.R. Sa de Melo, *Phys. Rev. Lett.* **99**, 080403 (2007); L.J. LeBlanc and J.H. Thywissen, *Phys. Rev. A* **75**, 053612 (2007); K. Sengupta, N. Dupuis, and P. Majumdar, *Phys. Rev. A* **75**, 063625 (2007); J.R. Williams, J.H. Huckans, R.W. Stites, E.L. Hazlett, and K.M. O'Hara, e-print arXiv:0804.2915v2 (20 April 2008).
- [78] K. Kirsten and D.J. Tom, *Phys. Rev. A* **54**, 4188 (1996).
- [79] D.J. Tom, *Annals Phys. (NY)* **320**, 487 (2005).
- [80] T. Haugset, H. Haugerud, and J.O. Andersen, *Phys. Rev. A* **55**, 2922 (1997).